THE JOURNAL OF PHYSICAL CHEMISTRY B
A JOURNAL OF THE AMERICAN CHEMICAL SOCIETY

pubs.acs.org/JPCB

Article

Analytical Calculation of the Elastic Moduli of Self-Assembled Liquid-Crystalline Bilayer Membranes

Xiaoyuan Wang, Sirui Li, and Yongqiang Cai*

Cite This: J. Phys. Chem. B 2021, 125, 5309−5320

Read Online

ACCESS | Metrics & More | Article Recommendations

ABSTRACT: Liquid-crystalline orders are ubiquitous in membranes and could significantly affect the elastic properties of the self-assembled bilayers. Calculating the free energy of bilayer membranes with different geometries and fitting them to their theoretical expressions allow us to extract the elastic moduli, such as the bending modulus and Gaussian modulus. However, this procedure is time-consuming for liquid-crystalline bilayers. In paper reports a novel method to calculate the elastic moduli of the self-assembled liquid-crystalline bilayers within the self-consistent field theory framework. Based on the asymptotic expansion method, we derive the analytical expression of the elastic moduli, which reduces the computational cost significantly. Numerical simulations illustrate the validity and efficiency of the proposed method.

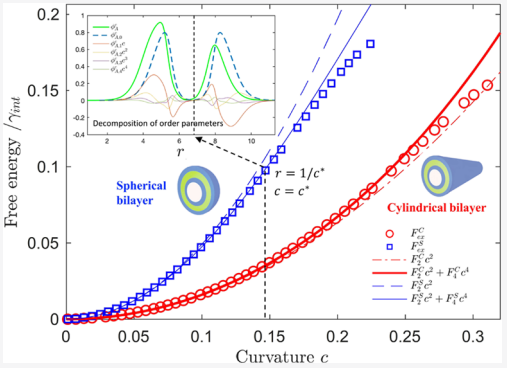

1. INTRODUCTION

Self-assembled bilayer membranes from amphiphilic molecules are abundant in biological and soft matter systems. Particularly, polymeric membranes have potential biomedicine and biotechnology applications due to their flexibility in the selection of monomers and chain architectures.[1] To use the membranes better, we need to understand their self-assembly and stability. Generally, the formation and stability of membrane morphologies can be understood by their mechanical properties. A membrane with negligible thickness could be modeled as a two-dimensional surface S. When the curvature is small, the deformation energy F of S could be described by the well-known Helfrich's linear elasticity theory[2,3]

$$F = \int_S [\gamma + 2\kappa_M(M - c_0)^2 + \kappa_G G]\mathrm{d}A \quad (1)$$

where M and G are the local mean and Gaussian curvatures of the deformed bilayer, respectively. The mechanical parameters are the surface tension γ, the spontaneous curvature c_0, the bending modulus κ_M, and the Gaussian modulus κ_G. Note that the spontaneous curvature c_0 is zero for bilayers due to its symmetry.

For membranes formed by the self-assembly of particular amphiphilic molecules, it is possible to study how the molecular architecture and parameters determine the elastic properties of the membranes. Particularly, experimental techniques,[4,5] simulation methods,[6−9] and theoretical analysis[10−12] have been developed to obtain the elastic moduli of membranes. A natural idea to extract the elastic moduli is studying bilayers in different geometries, such as planes, cylinders, and spheres, and then comparing their free energies with the corresponding expressions derived from elasticity theories.[11] In detail, there are two methods to do this: the polynomial fitting method (PFM) and the asymptotic expansion method (AEM). The PFM performs a computation of the free energy of curved membranes and then extracts the elastic constants by polynomial fitting of the theoretical expressions to the computed free energy curves.[11] The AEM regards the curvature of bilayers as a small parameter and carries out an asymptotic expansion of the free energy in terms of the curvature to derive analytical expressions for the elastic constants.[13]

Both the PFM and the AEM require accurate computation of the free energy of bilayer membranes. Among the different theoretical frameworks developed for amphiphilic molecules, the self-consistent field theory (SCFT) provides a versatile platform for studying self-assembled bilayer membranes. Several studies[14−17] using the SCFT have been carried out to study the elastic properties of bilayers by the PFM. Recently, Cai et al.[13] derived the AEM for flexible bilayers within the SCFT framework. In these studies, the polymers are assumed to be flexible, and the Gaussian polymer model is used to

Received: February 6, 2021
Revised: May 2, 2021
Published: May 14, 2021

https://doi.org/10.1021/acs.jpcb.1c01116
J. Phys. Chem. B 2021, 125, 5309−5320

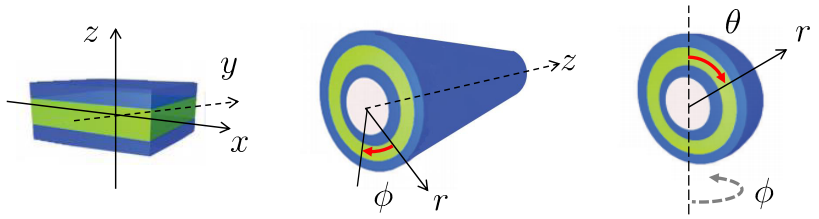

Figure 1. Three geometries: infinite planar, cylindrical, and spherical bilayers with a given curvature.

describe the blocks. Although many amphiphilic molecules contain a rigid or semiflexible component, the elastic properties for semiflexible bilayers are less explored. Cai et al.[18] extended the PFM to a semiflexible chain model described by the wormlike chain to study the elastic properties of liquid-crystalline bilayers and found that the liquid-crystalline order of the bilayers could have significant effects on the elastic properties of the membranes. Since the AEM could provide the analytical expression of elastic moduli and allows one to design more efficient numerical schemes,[13] it is valuable to extend the AEM to semiflexible bilayers and verify its numerical efficacy compared with the PFM.

Here, we perform the AEM on semiflexible bilayers that possess liquid-crystalline orders self-assembled from wormlike chains within the SCFT framework. It is well known that the self-assembly of semiflexible polymers is significantly different from that of the flexibility polymers even for the simple rod-coil systems.[19−23] For the semiflexible bilayers, it has been predicted that various liquid-crystalline orders, such as A phase and C-phase, could become equilibrium phases of the rod-coil/coil blends.[24] Numerically, the additional orientation dimensions of wormlike chains make the computation of liquid-crystalline bilayers time-consuming. This computational burden is aggravated when PFM is used to extract the elastic constants because the PFM needs to calculate the free energy of bilayers with many different curvatures. In this study, using the AEM, we analyze the excess free energy of bilayer membranes in three different geometries: an infinite planar bilayer; a cylindrical bilayer, which is extended to infinity in the axial direction; and a spherical bilayer with different curvatures (Figure 1). Specifically, we treat the curvature of cylindrical and spherical bilayers as small parameters and then carry out asymptotic expansions for the modified diffusion equation of propagators and order parameter of polymeric monomers in terms of the curvature, after which the self-consistent field (SCF) equations at each order can be derived. Finally, we can obtain analytical expressions of the free energy at each order, which are related to the elastic moduli and could be computed separately. Notably, a few SCF equations need to be solved to calculate these expanded free energies.

The remainder of this paper is organized as follows. Section 2 gives the SCFT model of semiflexible bilayers and two schemes to calculate the elastic moduli: the PFM and the AEM. Section 3 derives the AEM for liquid-crystalline bilayers. Section 4 presents the numerical method for solving the whole SCFT model. Numerical examples and comparisons of the two methods are illustrated in Section 5. Finally, Section 6 concludes with a brief summary.

2. THEORETICAL MODEL AND GEOMETRY CONSTRAINTS

2.1. Molecular Model. We consider the model system (used in ref 18) as a binary mixture of A(flexible)B-(semiflexible)-diblock copolymers and A-homopolymers. In this generic model, the amphiphilic molecules are modeled by the diblock copolymers and the amphiphilic solvent molecules are modeled by the homopolymers. To specify the model, we assume that the copolymers and homopolymers have the same degree of polymerization N and the volume fraction of the A and B blocks of the copolymers are f_A and $f_B = 1 - f_A$, respectively. In addition, the flexible chains are modeled as Gaussian chain and the semiflexible chains are modeled as the wormlike chain with a rigidity parameter λ. Based on the statistical segment lengths of A and B blocks (denoted by a and b, respectively), we define the geometrical asymmetry parameter[24−26] as $\beta = L/R_g$, where $L = bN$ is the total polymer contour and $R_g = \sqrt{Na^2/6}$ is the gyration radius. Furthermore, the Flory−Huggins parameter[27] χ and the Maier−Saupe parameter[28] η are used to describe the interaction between the A and B monomers and the orientation interaction between the semiflexible segments, respectively. Finally, the average concentration of the diblock copolymers is controlled by the activity z_c of the chemical potential. Within the SCFT framework formulated in the grand canonical ensemble, the free energy of our AB/hA system is given by[24]

$$\begin{aligned}\frac{N\mathcal{F}}{k_BT\rho_0} = \int d\mathbf{r}[&\chi N\phi_A(\mathbf{r})\phi_B(\mathbf{r}) - \omega_A(\mathbf{r})\phi_A(\mathbf{r}) \\ &- \omega_B(\mathbf{r})\phi_B(\mathbf{r}) \\ &+\frac{1}{2\eta N}\mathbf{M}(\mathbf{r}):\mathbf{M}(\mathbf{r}) - \xi(\mathbf{r})(\phi_A(\mathbf{r}) + \phi_B(\mathbf{r}) - 1) \\ &+\psi G_\varepsilon(\mathbf{r} - \mathbf{r}_1)(\phi_A(\mathbf{r}) - \phi_B(\mathbf{r}))] - z_cQ_c - Q_h\end{aligned} \quad (2)$$

where $\phi_A(\mathbf{r})$, $\phi_B(\mathbf{r})$ and $\omega_A(\mathbf{r})$, $\omega_B(\mathbf{r})$ are the local concentration and the mean field of the A and B monomers, respectively; $\mathbf{M}(\mathbf{r})$ is the mean orientation field of the semiflexible blocks; $\xi(\mathbf{r})$ is the Lagrange multiplier enforcing the incompressibility of the system; and ψ is another Lagrange multiplier introduced to stabilize the bilayer of different geometries.[16,18,29] Here, a sharp Gaussian function $G_\varepsilon(\mathbf{r} - \mathbf{r}_1)$ with width ε is used to ensure that the ψ field only operates near the interface at a prescribed position $\mathbf{r}_1$. In addition, Q_c and Q_h are the contributions from the single-chain partition functions of the copolymers and homopolymers.

The fundamental quantities to be calculated in the SCFT are the propagators that can be regarded as the probability distribution functions of polymer segments. In the presence of the mean fields ω_A, ω_B, and $\mathbf{M}$, the propagators $q_A^h(\mathbf{r}, s)$ for the A-homopolymers and $q_A^{\pm}(\mathbf{r}, s)$, $q_B^{\pm}(\mathbf{r}, \mathbf{u}, s)$ for the AB-diblock copolymers satisfy the modified diffusion equations (MDE)[30]

$$\frac{\partial}{\partial s}q_A^h(\mathbf{r}, s) = (R_g^2\nabla_{\mathbf{r}}^2 - \omega_A(\mathbf{r}))q_A^h(\mathbf{r}, s), \quad s \in (0, 1) \quad (3)$$

https://doi.org/10.1021/acs.jpcb.1c01116
J. Phys. Chem. B 2021, 125, 5309−5320

$$\frac{\partial}{\partial s}q_{\mathrm{A}}^{\pm}(\mathbf{r}, s) = (R_{\mathrm{g}}^2\nabla_{\mathbf{r}}^2 - \omega_{\mathrm{A}}(\mathbf{r}))q_{\mathrm{A}}^{\pm}(\mathbf{r}, s), \quad s \in (0, f_{\mathrm{A}}) \tag{4}$$

$$\frac{\partial}{\partial s}q_{\mathrm{B}}^{\pm}(\mathbf{r}, \mathbf{u}, s) = \left(\pm\beta R_{\mathrm{g}}\mathbf{u}\cdot\nabla_{\mathbf{r}}|_{\mathbf{u}} - \Gamma(\mathbf{r}, \mathbf{u}) + \frac{L}{2\lambda}\nabla_{\mathbf{u}}^2\right)q_{\mathrm{B}}^{\pm}(\mathbf{r}, \mathbf{u}, s), \quad s \in (0, f_{\mathrm{B}}) \tag{5}$$

with the initial conditions

$$q_{\mathrm{A}}^{\mathrm{h}}(\mathbf{r}, 0) = q_{\mathrm{A}}^{-}(\mathbf{r}, 0) = 1, \quad q_{\mathrm{B}}^{-}(\mathbf{r}, \mathbf{u}, 0) = \frac{1}{4\pi} \tag{6}$$

$$q_{\mathrm{A}}^{+}(\mathbf{r}, 0) = \int \mathrm{d}\mathbf{u}q_{\mathrm{B}}^{-}(\mathbf{r}, \mathbf{u}, f_{\mathrm{B}}), \quad q_{\mathrm{B}}^{+}(\mathbf{r}, \mathbf{u}, 0) = \frac{1}{4\pi}q_{\mathrm{A}}^{-}(\mathbf{r}, f_{\mathrm{A}}) \tag{7}$$

Here, $\mathbf{u}$ is a unit orientational vector and $\Gamma(\mathbf{r}, \mathbf{u})$ is an $\mathbf{r}$, $\mathbf{u}$-dependent field defined as $\Gamma(\mathbf{r}, \mathbf{u}) = \omega_{\mathrm{B}}(\mathbf{r}) - \mathbf{M}(\mathbf{r})$: $(\mathbf{uu} - 1/3\mathbf{I})$. In terms of the chain propagators, the single-chain partition functions are calculated by $Q_{\mathrm{c}} = \int \mathrm{d}\mathbf{r}q_{\mathrm{A}}^{+}(\mathbf{r}, f_{\mathrm{A}})$, $Q_{\mathrm{h}} = \int \mathrm{d}\mathbf{r}q_{\mathrm{A}}^{\mathrm{h}}(\mathbf{r}, 1)$, the local concentration of the A and B monomers are obtained by

$$\begin{aligned}\phi_{\mathrm{A}}(\mathbf{r}) &= \phi_{\mathrm{A}}^{\mathrm{h}} + \phi_{\mathrm{A}}^{\mathrm{c}} \\ &= \int_0^1 \mathrm{d}s q_{\mathrm{A}}^{\mathrm{h}}(\mathbf{r}, s)q_{\mathrm{A}}^{\mathrm{h}}(\mathbf{r}, 1 - s) \\ &\quad + z_{\mathrm{c}}\int_0^{f_{\mathrm{A}}} \mathrm{d}s q_{\mathrm{A}}^{-}(\mathbf{r}, s)q_{\mathrm{A}}^{+}(\mathbf{r}, f_{\mathrm{A}} - s)\end{aligned} \tag{8}$$

$$\phi_{\mathrm{B}}(\mathbf{r}) = 4\pi z_{\mathrm{c}}\int_0^{f_{\mathrm{B}}} \mathrm{d}s \int \mathrm{d}\mathbf{u}q_{\mathrm{B}}^{-}(\mathbf{r}, \mathbf{u}, s)q_{\mathrm{B}}^{+}(\mathbf{r}, \mathbf{u}, f_{\mathrm{B}} - s) \tag{9}$$

and the orientational order parameter of the B blocks is given by

$$\mathbf{S}(\mathbf{r}) = 4\pi z_{\mathrm{c}}\int_0^{f_{\mathrm{B}}} \mathrm{d}s \int \mathrm{d}\mathbf{u}q_{\mathrm{B}}^{-}(\mathbf{r}, \mathbf{u}, s)\left(\mathbf{uu} - \frac{\mathbf{I}}{3}\right)q_{\mathrm{B}}^{+}(\mathbf{r}, \mathbf{u}, f_{\mathrm{B}} - s) \tag{10}$$

Finally, the mean fields and the local concentrations are linked by the SCF equations

$$\omega_{\mathrm{A}}(\mathbf{r}) = \chi N\phi_{\mathrm{B}}(\mathbf{r}) - \xi(\mathbf{r}) + \psi G_{\varepsilon}(\mathbf{r} - \mathbf{r}_1) \tag{11}$$

$$\omega_{\mathrm{B}}(\mathbf{r}) = \chi N\phi_{\mathrm{A}}(\mathbf{r}) - \xi(\mathbf{r}) - \psi G_{\varepsilon}(\mathbf{r} - \mathbf{r}_1) \tag{12}$$

$$\mathbf{M}(\mathbf{r}) = \eta\mathbf{N}\mathbf{S}(\mathbf{r}) \tag{13}$$

$$\phi_{\mathrm{A}}(\mathbf{r}) + \phi_{\mathrm{B}}(\mathbf{r}) = 1 \tag{14}$$

$$\int \mathrm{d}\mathbf{r}G_{\varepsilon}(\mathbf{r} - \mathbf{r}_1)(\phi_{\mathrm{A}}(\mathbf{r}) - \phi_{\mathrm{B}}(\mathbf{r})) = 0 \tag{15}$$

Eqs 2−15 form the whole SCFT model. Although the SCF equations could have many solutions due to its high nonlinearity, we focus on the solutions corresponding to liquid-crystalline bilayers. Furthermore, the free energy of a bilayer is compared to that of the homogeneous bulk phase $\mathcal{F}_{\mathrm{bulk}}$, which can be computed analytically.[16,24,31] Since the free energy difference $(\mathcal{F} - \mathcal{F}_{\mathrm{bulk}})$ is proportional to the area of membrane A, we can define an excess free energy density by

$$F_{\mathrm{ex}} = \frac{N(\mathcal{F} - \mathcal{F}_{\mathrm{bulk}})}{k_{\mathrm{B}}T\rho_0 A} \tag{16}$$

which will be compared with the deformation energy of bilayers given in eq 1.

2.2. Geometric Constraints and the PFM. To extract the bending modulus and Gaussian modulus of the self-assembled bilayers, one can calculate the excess free energy of bilayer membranes in three geometries:[11,16,18] an infinite plane, a cylinder, and a sphere. These geometries are easy to simulate since we can reduce the computation domain to dimension one in their corresponding coordinate systems. Furthermore, MDEs 3−5 are now in one-dimensional planar, cylindrical, and spherical coordinate systems, which can be written in unified forms[18] (omit the superscripts and subscripts)

$$\frac{\partial}{\partial s}q(r, s) = a^2\left(\frac{\partial^2}{\partial r^2} + \frac{n}{r}\frac{\partial}{\partial r}\right)q(r, s) - \omega(r)q(r, s) \tag{17}$$

$$\frac{\partial}{\partial s}q(r, \mathbf{u}, s) = (L_{\mathrm{P}} \pm \frac{\beta}{r}L_{\mathrm{CS}})q(r, \mathbf{u}, s) \tag{18}$$

where $L_{\mathrm{P}} = \pm\beta\cos\Theta\partial_r - \Gamma(\mathbf{r}, \mathbf{u}) + \frac{1}{2\lambda}\nabla_{\mathbf{u}}^2$ is the operator corresponding to planar bilayer, L_{CS} is an operator introduced by cylindrical or spherical deformations

$$L_{\mathrm{CS}} = \begin{cases} 0, & n = 0 \\ \cos\Theta\sin\Phi\cos\Phi\partial_\Phi - \sin\Theta\cos^2\Phi\partial_\Theta =: L_{\mathrm{C}}, & n = 1 \\ -\sin\Theta\partial_\Theta =: L_{\mathrm{S}}, & n = 2 \end{cases}$$

and n = 0, 1, and 2 for planar, cylindrical, and spherical coordinate systems, respectively. Here, Θ and Φ in operators L_{CS} are the local orientational angle of $\mathbf{u}$ in the cylindrical or spherical coordinate systems.

In the cylindrical and spherical geometries, the constraint $\psi G_{\varepsilon}(\mathbf{r} - \mathbf{r}_1)$ in eq 2 applied to the outer monolayer, where $\mathbf{r}_1$ is set to control the curvature c of the self-assembled bilayer. With these constraints, the obtained excess free energies for the three geometries, F^0, $F^{\mathrm{C}}(c)$, and $F^{\mathrm{S}}(c)$, are compared with the theoretical free energies

$$F^0 = \gamma + 2\kappa_{\mathrm{M}}c_0^2 \tag{19}$$

$$F^{\mathrm{C}}(c) = F^0 - 2\kappa_{\mathrm{M}}c_0c + \frac{\kappa_{\mathrm{M}}}{2}c^2 + B_{\mathrm{C}}c^4 + \ldots \tag{20}$$

$$F^{\mathrm{S}}(c) = F^0 - 4\kappa_{\mathrm{M}}c_0c + (2\kappa_{\mathrm{M}} + \kappa_{\mathrm{G}})c^2 + B_{\mathrm{S}}c^4 + \ldots \tag{21}$$

where the high-order moduli, such as B_{C} and B_{S}, are introduced for medium or large curvatures. Since the energies $F^{\mathrm{C}}(c)$ and $F^{\mathrm{S}}(c)$ are polynomials when the curvature c is small, their coefficients can be extracted from two datasets, $\{(c_i, F^{\mathrm{C}}(c_i))\}$ and $\{(c_i, F^{\mathrm{S}}(c_i))\}$, by the standard polynomial fitting method.[16,18] Here, for each curvature c_i in the set $\{c_i\}$, the free energy $F(c_i)$ ($F^{\mathrm{C}}(c_i)$ or $F^{\mathrm{S}}(c_i)$) is calculated by solving the SCFT model with the geometric constraint at $\mathbf{r}_1$ corresponding to c_i.

2.3. AEM. Taking the curvature c of cylindrical and spherical bilayers as small parameters in the asymptotic expansion theory,[32,33] we can get asymptotic expansions for the SCFT model. Denote $x = r - 1/c$ as the local coordinate

https://doi.org/10.1021/acs.jpcb.1c01116
J. Phys. Chem. B 2021, 125, 5309−5320

using the location of bilayer as a reference, then we can expand $1/r$ as

$$\frac{1}{r} = \frac{1}{x + 1/c} = \frac{c}{1 + cx} = c - xc^2 + x^2c^3 + ... \tag{22}$$

The propagators, local concentrations and mean fields can be expanded accordingly. We add a subscript i to denote the ith-order term in the asymptotic expansion. For example, q_{Ai} is the ith term of the expansion for $q_A(r, s)$

$$q_A(r, s) = q_{A0}(x, s) + cq_{A1}(x, s) + c^2q_{A2}(x, s) + ...$$

Furthermore, analytic expressions of the MDE and SCF equations at each order could be obtained separately, which is established in Section 3 for liquid-crystalline bilayers.

Once we solved the expanded SCF equations, the free energy of a bilayer at each order can be analytically expressed. Denoting the expansion for the semilocal excess energy density by $f(r) = \sum_{i\geq 0} c^i f_i(x)$, we have the expansion for the excess energy density F_{ex}

$$\begin{aligned} F_{ex} &= \frac{1}{A}\int_V f(\mathbf{r})d\mathbf{r} = c^n \int_0^\infty r^n f(r)dr \\ &= \int_{-1/c}^\infty (1 + cx)^n (f_0(x) + cf_1(x) + c^2f_2(x) + ...)dx \\ &= \sum_{i\geq 0} c^i \int_{-\infty}^\infty dx \sum_{j=0}^i p_j(x) f_{i-j}(x) =: \sum_{i\geq 0} c^i F_i \end{aligned} \tag{23}$$

where the functions $p_j(x)$ are monomials from the binomial expansion of $(1 + cx)^n$

$$p_0(x) = 1, \quad p_1(x) = nx, \quad p_2(x) = \frac{n(n-1)}{2}x^2, \quad ...$$

Since we only consider $n = 0$, 1, and 2, we have $p_j(x) = 0$ for $j > 2$. By eq 23, we have the ith-order free energy of F_{ex}

$$F_i = \int_{-\infty}^\infty dx \sum_{j=0}^i p_j(x) f_{i-j}(x) \tag{24}$$

In particular, we have the first three terms from the free energy expansion

$$F_0 = \int_{-\infty}^\infty f_0(x)dx \tag{25}$$

$$F_1 = \int_{-\infty}^\infty (f_1(x) + nxf_0(x))dx \tag{26}$$

$$F_2 = \int_{-\infty}^\infty \left(f_2(x) + nxf_1(x) + \frac{n(n-1)}{2}x^2 f_0(x)\right)dx \tag{27}$$

Denote the free energy of cylindrical and spherical bilayers (corresponding to $n = 1$ and 2, respectively) at ith order as F_i^C and F_i^S, then the elastic moduli can be directly calculated

$$\begin{aligned} &\kappa_M = 2F_2^C, \quad \kappa_G = F_2^S - 4F_2^C, \\ &c_0 = -F_1^C/(2\kappa_M) = -F_1^S/(4\kappa_M), \quad \gamma = F_0 - 2\kappa_M c_0^2 \end{aligned} \tag{28}$$

Compared with the PFM, the AEM analytically gives the elastic moduli corresponding to a series of SCF equations. Our previous study[13] derived these MDE and SCF equations for flexible bilayers. In the next sections, we extend the AEM to the liquid-crystalline bilayers and design numerical methods to solve the obtained equations.

3. AEM FOR LIQUID-CRYSTALLINE BILAYERS

Compared with the flexible bilayers, the semiflexible bilayers could have liquid-crystalline orders which have significant effects on the bilayers' phase behavior and elastic property. Here, we derive the analytical expression of the elastic moduli for liquid-crystalline bilayers. In particular, we focus on the A phase bilayers for which the MDE of rods in cylindrical and spherical coordinate systems have a unified form eq 18. To use the AEM, we need to expand the MDEs with respect to the curvature; then, the SCF equation and free energy at each order can be derived.

3.1. MDEs at Each Order. For flexible Gaussian chains, the MDE has the form of eq 17. According to the asymptotic expansion for field ω and propagator q in eq 17, we have

$$\begin{aligned} &(a^2\nabla^2 - \omega(r))q(r, s) \\ &= \left(a^2\partial_{rr} + \frac{na^2}{r}\partial_r - \omega_0(x) - c\omega_1(x) - c^2\omega_2(x) + ...\right) \\ &\times (q_0(x, s) + cq_1(x, s) + c^2q_2(x, s) + ...) \end{aligned} \tag{29}$$

Substituting the relation 22 of r and x into eq 29 and comparing the terms with different orders of c, we get the MDE at the ith order

$$\partial_s q_i(x, s) = (a^2\partial_{xx}^2 - \omega_0)q_i(x, s) + g_i(x, s) \tag{30}$$

where $g_i(x, s)$ is a source term independent of $q_i(x, s)$

$$g_i(x, s) = \sum_{j=1}^i (na^2(-x)^{j-1}\partial_x - \omega_j)q_{i-j}(x, s) \tag{31}$$

For wormlike chains, the MDE has the form of eq 18. Substituting the asymptotic expansion for field Γ and propagator q into eq 18, we have

$$\begin{aligned} &\left(\pm\beta(\cos\Theta\partial_r + \frac{1}{r}L_{CS}\right) - \Gamma(\mathbf{r}, \mathbf{u}) + \frac{1}{2\lambda}\nabla_{\mathbf{u}}^2)q^{\pm}(\mathbf{r}, \mathbf{u}, s) \\ &= \Big[\pm\beta(\cos\Theta\partial_x + (c - xc^2 + x^2c^3 + ...)L_{CS}) \\ &\quad - (\Gamma_0(x, \mathbf{u}) + c\Gamma_1(x, \mathbf{u}) + c^2\Gamma_2(x, \mathbf{u}) + ...) + \frac{1}{2\lambda}\nabla_{\mathbf{u}}^2\Big] \\ &\times (q_0^{\pm}(x, \mathbf{u}, s) + cq_1^{\pm}(x, \mathbf{u}, s) + c^2q_2^{\pm}(r, \mathbf{u}, s) + ...) \end{aligned}$$

Expanding these terms and comparing them with different orders of c, we get

$$\partial_s q_i^{\pm}(x, \mathbf{u}, s) = L_P q_i^{\pm}(x, \mathbf{u}, s) + g_i(x, \mathbf{u}, s) \tag{32}$$

where $L_P = \pm\beta\cos\Theta\partial_x - \Gamma_0(x, \mathbf{u}) + \frac{1}{2\lambda}\nabla_{\mathbf{u}}^2$ is the derivative operator corresponding to planar bilayers and $g_i(x, \mathbf{u}, s)$ is the source term defined as

$$g_i(x, \mathbf{u}, s) = \sum_{j=1}^i (\pm\beta(-x)^{j-1}L_{CS} - \Gamma_j(x, \mathbf{u}))q_{i-j}^{\pm}(x, \mathbf{u}, s) \tag{33}$$

https://doi.org/10.1021/acs.jpcb.1c01116
J. Phys. Chem. B 2021, 125, 5309−5320

3.2. SCF Equation and Free Energy at Each Order. For the AB/hA model system, the MDEs eqs 30 and 32 for $q^{\pm}_{Ai}$, $q^{\pm}_{Bi}$, and q^{h}_{Ai} have the following initial conditions

$$q^{h}_{A0}(x, 0) = q^{-}_{A0}(x, 0) = 1, \quad q^{-}_{B0}(x, \mathbf{u}, 0) = \frac{1}{4\pi},$$

$$q^{h}_{Ai}(x, 0) = q^{-}_{Ai}(x, 0) = 0,$$
$$q^{-}_{Bi}(x, \mathbf{u}, 0) = 0, i = 1, 2, ...,$$

$$q^{+}_{Ai}(x, 0) = \int d\mathbf{u} q^{-}_{Bi}(x, \mathbf{u}, f_B),$$
$$q^{+}_{Bi}(x, \mathbf{u}, 0) = \frac{1}{4\pi} q^{-}_{Ai}(x, f_A), i = 0, 1, 2, ...$$

After solving the MDEs, we can calculate the expansions at each order for order parameters $\phi^{h}_{A}(x)$, $\phi^{c}_{A}(x)$, $\phi^{c}_{B}(x)$, and $\mathbf{S}(x)$. For example

$$\mathbf{S}(x) = \sum_{i\geq 0} c^i \mathbf{S}_i(x) = \sum_{i\geq 0} c^i 4\pi z_c \int_0^{f_B} ds \int d\mathbf{u} \sum_{j=0}^{i} q^{-}_{Bj}(x, \mathbf{u}, s)\left(\mathbf{uu} - \frac{\mathbf{I}}{3}\right) q^{+}_{B,i-j}(x, \mathbf{u}, f_B - s) \tag{34}$$

The SCF equations can be done similarly. In the geometric constraint $\psi G_\varepsilon(\mathbf{r} - \mathbf{r}_1)$, the position r_1 can be decomposed as $r_1 = 1/c + (r_1 - 1/c) =: 1/c + h$, where $1/c$ is the radius of the cylindrical or spherical bilayer and $h := r_1 - 1/c$ is the relative position of the constraint. Instead of using r_1 explicitly, we use its relative position h, which is determined by the equation

$$\int_{-\infty}^{\infty} G_\varepsilon(x - h)(\phi_{A0}(x) - \phi_{B0}(x))dx = 0 \tag{35}$$

Denoting the expansion of the relative position by $h = \sum_{i\geq 0} c^i h_i$ and using the Taylor expansion of $G_\varepsilon(x - h)$, we get

$$G_\varepsilon(x - h) = \sum_{k\geq 0} \frac{(h_0 - h)^k}{k!} G^{(k)}_\varepsilon(x - h_0) = \sum_{k\geq 0} \frac{\left(-\sum_{i\geq 1} c^i h_i\right)^k}{k!} G^{(k)}_\varepsilon(x - h_0) = \sum_{i\geq 0} c^i G_{\varepsilon,i}(x - h_0)$$

Considering the expansion of the Lagrange multiplier $\xi(r) = \sum_{i\geq 0} c^i \xi_i(x)$ and the constraint field $\psi = \sum_{i\geq 0} c^i \psi_i$ and comparing the eqs 11−15 at each order, we have the SCF equations for the liquid-crystalline bilayer at the ith order

$$\omega_{Ai}(x) = \chi N \phi_{Bi}(x) - \xi_i(x) + \sum_{j=0}^{i} \psi_j G_{\varepsilon,i-j}(x - h_0) \tag{36}$$

$$\omega_{Bi}(x) = \chi N \phi_{Ai}(x) - \xi_i(x) - \sum_{j=0}^{i} \psi_j G_{\varepsilon,i-j}(x - h_0) \tag{37}$$

$$\mathbf{M}_i(x) = \eta N \mathbf{S}_i(x) \tag{38}$$

$$\phi_{Ai}(x) + \phi_{Bi}(x) = \delta_{0i} \tag{39}$$

$$\int_{-\infty}^{\infty} \sum_{j=0}^{i} G_{\varepsilon,j}(x - h_0) \sum_{k=0}^{i-j} p_k(x)(\phi_{A,i-j-k}(x) - \phi_{B,i-j-k}(x)) dx = 0 \tag{40}$$

Here, $\delta_{00} \equiv 1$ for $i = 0$, and $\delta_{0i} \equiv 0$ for $i \geq 1$. It should be noted that there is no constraint to stabilize the planar bilayers; hence, we have $\psi_0 = 0$. Finally, the SCF equations are closed after the curvature c of the bilayer is determined. For a curved bilayer of finite thickness, the definition of the interface position is somewhat arbitrary. Following our previous setting,[13] we define the curvature of cylindrical and spherical bilayers as c satisfying $\int(|\mathbf{r}| - 1/c)\rho(\mathbf{r})d\mathbf{r} = \int_0^\infty r^n(r - 1/c)\rho(r)dr = 0$, where $\rho(\mathbf{r}) := \phi_B(\mathbf{r}) - f_B\phi_{bulk}$ is regarded as a density function and ϕ_{bulk} is the bulk copolymer concentration. Expanding $\rho(\mathbf{r})$ as $\rho(\mathbf{r}) = \sum_{i\geq 0} c^i \rho_i(x)$, we have the following constraints

$$I_{\psi,i} := \sum_{j=0}^{i} \int_{-\infty}^{\infty} x p_j(x) \rho_{i-j}(x) dx = 0, \quad i = 0, 1, 2, ... \tag{41}$$

In summary, the SCF equations for $i \geq 1$ are eqs 36−41. The value of h is calculated from eq 35 after the SCF equation for $i = 0$ is solved. Once we solved the SCF equations at each order (see Section 4 for the numerical methods), the free energy of a bilayer can be calculated analytically. For AB/hA systems, the semilocal excess energy density $f(r)$ is $f(r) = f_{bilayer}(r) - f_{bulk}$, where f_{bulk} is the energy density of the bulk phase. Using the expansion in eq 23, we have the ith component of $f(x)$ giving by

$$f_i(x) = \sum_{k=0}^{i} [\chi N \phi_{A,k}(x)\phi_{B,i-k}(x) - \omega_{A,k}(x)\phi_{A,i-k}(x) - \omega_{B,k}(x)\phi_{B,i-k}(x) + \frac{1}{2\eta N}\mathbf{M}_k(\mathbf{r}) : \mathbf{M}_{i-k}(\mathbf{r})] - z_c q^{+}_{A,i}(x, f_A) - q^{h}_{A,i}(x, 1) - \delta_{0i} f_{bulk}$$

Then, the elastic moduli can be calculated by eqs 25−27. Note that for flexible bilayers, our previous study[13] shows that $F^0 = F^C_0 = F^S_0$ and $2F^C_1 = F^S_1$. These relations are also true for liquid-crystalline bilayers since the zeroth-order SCF equations are the same as that of the planar bilayers and the first-order SCF equations for cylindrical and spherical bilayers only have a different scale n.

4. NUMERICAL METHOD

In this section, we turn to the numerical method to solve the SCF equations. Generally, the SCFT models can be solved by iteration methods. In solving SCF equations, we need to solve the MDE, which is the most time-consuming step, especially for semiflexible chains. For the AEM, the SCF equations at each order are solved successively, then the free energy and structure of the bilayers at each order can be obtained.

4.1. Solve the MDEs for the AEM. Unlike the PFM that should solve MDEs in eqs 17 and 18, the MDEs in the AEM are eqs 30 and 32 where the main difference is the source terms g_i. Our previous work[13] developed the numerical method for solving MDE of coils; therefore, here, we only give the numerical method for MDE of rods, *i.e.*, eq 32. Furthermore,

https://doi.org/10.1021/acs.jpcb.1c01116
J. Phys. Chem. B 2021, 125, 5309−5320

we reformulate eq 32 with initial value q^0 and a reflection bound condition as

$$\frac{\partial}{\partial s}q(x, \mathbf{u}, s) = a\frac{\partial}{\partial x}q(x, \mathbf{u}, s) - \Gamma_0(x, \mathbf{u})q(x, \mathbf{u}, s) + \frac{1}{2\lambda}\nabla_{\mathbf{u}}^2 q(x, \mathbf{u}, s) + g(x, \mathbf{u}, s) \tag{42}$$

$$q(x, \mathbf{u}, 0) = q^0(x, \mathbf{u}), \quad \frac{\partial}{\partial x}q(x_{\text{in}}, \mathbf{u}, s) = 0 \tag{43}$$

where $g(x, \mathbf{u}, s)$ is a given source term. The computational domain is truncated to a proper interval $[-L, L]$ with length $2L$, and the boundary condition is at $x_{\text{in}} = \pm L$ (the sign is assigned from the sign of the coefficient a).

To capture the sharp interface of bilayers, we employ nonuniform grids corresponding to a given monotone function $x = t(\zeta)$ satisfying $t(\pm L) = \pm L$, $t''(\pm L) = 0$ (a valid choice is given in Appendix A). Then, with a proper change of variables, $q(x, s) = \sqrt{t'(\zeta)}\,u(\zeta, s)$, eq 42 will be changed but has the same form except variable coefficients and the source term

$$\frac{\partial}{\partial s}u(\zeta, \mathbf{u}, s) = \tilde{a}(\zeta)\frac{\partial}{\partial \zeta}u(\zeta, \mathbf{u}, s) - \tilde{\Gamma}_0(\zeta, \mathbf{u})u(\zeta, \mathbf{u}, s) + \frac{1}{2\lambda}\nabla_{\mathbf{u}}^2 u(\zeta, \mathbf{u}, s) + \tilde{g}(\zeta, \mathbf{u}, s) \tag{44}$$

$$u(\zeta, \mathbf{u}, 0) = u^0(\zeta, \mathbf{u}), \quad \frac{\partial}{\partial \zeta}u(\zeta_{\text{in}}, \mathbf{r}, s) = 0 \tag{45}$$

where the new coefficients are

$$\tilde{a}(\zeta) = \frac{a}{t'(\zeta)}, \quad \tilde{\Gamma}_0(\zeta, \mathbf{u}) = \Gamma_0(t(\zeta), \mathbf{u}) - \frac{at''}{2t'^2(\zeta)},$$
$$\tilde{g}(\zeta, \mathbf{u}, s) = \frac{1}{\sqrt{t'(\zeta)}}g(t(\zeta), \mathbf{u}, s)$$

Employing the well-known Strang split method,[34] we obtain the following two-order semidiscrete scheme for eq 44 with step size Δs

$$u^{k+1/2}(\zeta, \mathbf{u}) = \exp[-\tilde{\Gamma}_0(\zeta, \mathbf{u})\frac{\Delta s}{2}) \left[u^k(\zeta, \mathbf{u}) + \frac{\Delta s}{8}(3\tilde{g}(\zeta, \mathbf{u}, s_k) + \tilde{g}(\zeta, \mathbf{u}, s_{k+1})\right],$$

$$u^*(\zeta, \mathbf{u}) = \exp(\tilde{a}(\zeta)\frac{\Delta s}{2}\partial_\zeta)u^{k+1/2}(\zeta, \mathbf{u}),$$

$$u^{\#}(\zeta, \mathbf{u}) = \exp(\nabla_{\mathbf{u}}^2\frac{\Delta s}{2\lambda})u^*(\zeta, \mathbf{u}),$$

$$u^{**}(\zeta, \mathbf{u}) = \exp(\tilde{a}(\zeta)\frac{\Delta s}{2}\partial_\zeta)u^{\#}(\zeta, \mathbf{u}),$$

$$u^{k+1}(\zeta, \mathbf{u}) = \exp(-\tilde{\Gamma}_0(\zeta, \mathbf{u})\frac{\Delta s}{2})u^{**}(\zeta, \mathbf{u}) + \frac{\Delta s}{8}(\tilde{g}(\zeta, \mathbf{u}, s_k) + 3\tilde{g}(\zeta, \mathbf{u}, s_{k+1}))$$

where $u^k(\zeta, \mathbf{u})$ is the numerical approximation of $u(\zeta, \mathbf{u}, s_k)$, $s_k = k\Delta s$. Here, $u^*(\zeta, \mathbf{u})$ and $u^{**}(\zeta, \mathbf{u})$ can be solved by the well-known Crank−Nicolson scheme,[35] and $u^{\#}(\zeta, \mathbf{u})$ can be solved by the spectral method employing the spherical harmonics $Y_l^m(\Theta, \Phi)$ as basic functions. Note that the source term $g_i(x, \mathbf{u}, s)$ (or its variant $\tilde{g}_i(\zeta, \mathbf{u}, s)$) is given by eq 33, whose evaluation is straightforward and can be numerically implemented by the spherical harmonics, *i.e.*, the operation of L_{CS} on a spherical harmonic can be expressed by several spherical harmonics (see Appendix B). It is worth noting that there are higher-order numerical schemes to solve the differential eqs 42 and 44. For instance, if the derivative operators on x (or ζ) are discretized by fourth-order compact finite difference schemes[36] and the derivative operators on s are discretized by fourth-order Runge−Kutta methods,[37] then one could obtain fourth-order schemes finally.

4.2. Solve the SCF Equations. The SCF equations can be solved by the Picard iteration, where the fields $\omega_{\text{A}i}$, $\omega_{\text{B}i}$, and $\mathbf{M}_i$ are updated from an old set of field, $\omega_{\text{A}i}^{\text{old}}(x)$, $\omega_{\text{B}i}^{\text{old}}(x)$, and $\mathbf{M}_i^{\text{old}}(x)$. In detail, we first solved the MDEs with these old mean fields to get propagators, $q_{\text{A}i}^{\pm}$, $q_{\text{B}i}^{\pm}$, and $q_{\text{A}i}^{\text{h}}$, which are directly used to calculate the order parameters $\phi_{\text{A}i}(x)$, $\phi_{\text{B}i}(x)$, and $\mathbf{S}_i(x)$. Next, we assign the Lagrange fields ξ_i and ψ_i according to eqs 39−4141. Then, the fields $\omega_{\text{A}i}$, $\omega_{\text{B}i}$, and $\mathbf{M}_i$ are updated according to eqs 3637−38. Repeat these steps until the error of SCF equations is small enough; then, the ith-order free energy can be obtained by eq 24. Detailed iteration formula is given in Appendix C. Note that the Picard iteration for SCF equations is robust but converges slowly. Hence, we use the Anderson mixing technique[38] of general fixed point problems to accelerate the convergence when the fields are updated by lots of Picard iterations.

4.3. Programming Skills. Now we introduce the programming aspect of the AEM. At first glance, our analytical approach seems cumbersome because there are many symbols with subscripts corresponding to different orders of the expansion. However, the programming is not cumbersome since we use the object-oriented programming (OOP), which treats the fields, order parameters, and propagators at each order as object instances of a same class. The main difference from solving planar bilayer SCF equations is that the MDE now has an additional source term, and the cross-multiplying terms are replaced by a for-loop summation (it is easy to implement using OOP). The main disadvantage is that we need to store the quantities of all orders, which consumes 5 times of CPU memory (*i.e.*, five object instances from the zeroth to the fourth orders of the fields, order parameters, and propagators) if we want to calculate the fourth-order elastic modulus. This is painless for flexible bilayers[13] but expected to be avoided for liquid-crystalline bilayers because the additional orientation dimensions will increase the CPU memory. Next, we introduce a trick to reduce the CPU memory to 2 times.

The main part of the memory consumption is that the propagator of each order needs to be restored for the subsequent calculations. For example, evaluating the source term $g_i(x, \mathbf{u}, s)$ by eq 33 will use the propagators q_0, ..., q_{i-1}. Since the propagators up to the $(i-1)$th order are only used but not modified, we can save them to the hard disk instead of to the CPU memory and load them back into the CPU memory when needed. Besides, the source term (except a tractable term $\Gamma_i(x, \mathbf{u})\, q_0^{\pm}$) is unchanged during the SCF iteration. Therefore, it is only once that we need to load the propagators from the hard disk back into the CPU memory to calculate the source term. Using this trick, we only need the CPU memory to store two object instances: one instance for the current order (ith-order fields, order parameters, and

https://doi.org/10.1021/acs.jpcb.1c01116
J. Phys. Chem. B 2021, 125, 5309−5320

propagators) and another instance for the accumulated terms (from the zeroth to the $(i-1)$th orders).

5. RESULTS AND DISCUSSION

In this section, we present some numerical examples of the AEM for tensionless liquid-crystalline bilayers, *i.e.*, the activity of chemical potential z_c is adjusted such as the planar bilayer has zero surface tension ($\gamma = 0$). The computational domain $[-L, L]$ is determined by the concentration profile to ensure the order near the boundary is close to the bulk phase. The orientational vector $\mathbf{u}$ on unit sphere is discretized by 32 values of Θ and 36 values of Φ, and the spherical harmonics Y_l^m for calculating $L_{CS}q$ is truncated by $|m| \le l \le 16$. The number of spatial and contour grid point are set as $N_x = 400$ and $N_s = 800$, respectively. The free energy is convergent in the order of 10^{-4}, and the fields are self-consistent with L^2-norm error less than 10^{-6}. The Gaussian width ε in eq 2 is set as $\varepsilon = 0.2R_g$. For the obtained elastic moduli, we use the unit same with Li et al.,[16] where the referenced length is $d = 4.3R_g$ and the interfacial free energy per unit area between coexisting A and B homopolymers (in the limit of large χN) is $\gamma_{int} = \sqrt{\chi N/6}\rho_0 k_B T a/\sqrt{N}$.

5.1. Compare the PFM and the AEM. To compare the PFM and the AEM, we first verify the consistency of the AEM with the directly constrained cylindrical and spherical bilayers. We show the energy curves in Figure 2 with model parameters

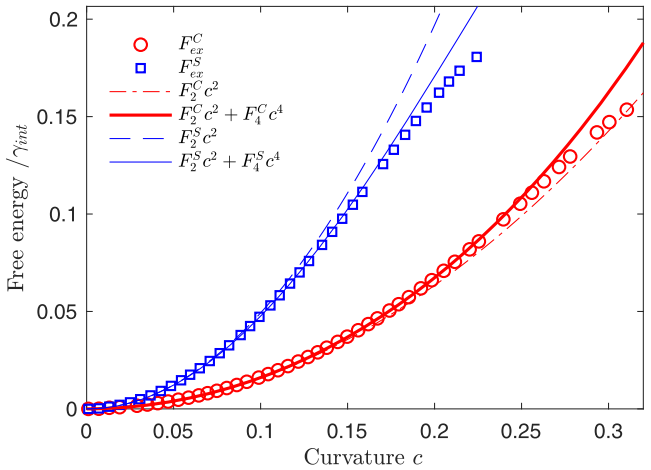

Figure 2. Comparison of the free energies of cylindrical and spherical bilayers. F_{ex} is calculated by the geometry constraint method, while F_2 and F_4 are calculated by the AEM. (Model parameters are $\chi N = 15$, $\eta N = 30$, $f_A = 0.5$, $\beta = 1$, and $\lambda/L = \infty$).

$\chi N = 15$, $\eta N = 30$, $f_A = 0.5$, $\beta = 1$, and $\lambda/L = \infty$. The circles and squares are the excess free energy of cylindrical and spherical bilayers calculated in the cylindrical and spherical coordinate systems, respectively.[18] Under this model parameter, the bilayer is self-assembled to A phase and its thickness is about $2.2R_g$ when the bilayer is slightly curved. Therefore, the curvature of spherical and cylindrical bilayers has an upper bound $c_{max} \sim 1/2.2 \approx 0.45$. Actually, numerical results reveal that the solution of the SCFT model with constrained curvature $c > c_{max} \approx 0.2$ for spheres (or $c_{max} \approx 0.3$ for cylinders) will tend to micelles instead of perfect bilayers. The solid and dashed energy curves in Figure 2 are the polynomials whose coefficients are determined by the AEM. It is obvious that the free energy from the AEM is consistent with that of the directly constrained simulations, which implies the consistency between the AEM and the PFM, *i.e.*, the second-order energy expansion F_2c^2 approximates $F_{ex}(c)$ well when the curvature c is small and adding the fourth-order energy F_4c^4 will improve the approximation for more larger curvatures. It is interesting to note that the fourth-order energy is positive for cylindrical bilayers but negative for spherical bilayers, *i.e.*, $F_4^C > 0$, $F_4^S < 0$. This trend occurs for most flexible bilayers[13,16] and semiflexible bilayers (see Section 5.3). It provides a qualitative understanding for highly curved membranes as the fourth-order energies become observable when the curvature is large. A similar result has been observed in molecular dynamic simulations of lipid models,[39] where the parabolic membrane stiffens with increasing curvature.

Now we consider the aspect of time cost. Generally, the total CPU time T for solving the SCFT model can be estimated by $T = Kt + T_0$, where K is the number of SCF iterations to converge, t is the time cost of one iteration, and T_0 is the warmup time. Since the total iteration number K depends on many factors, such as the quality of initial guess of fields, the stopping criteria, and the iteration schemes, we only compare the time cost t and T_0. In the AEM, T_0 is the CPU time to calculate the source terms at the beginning of iterations. Figure 3 shows the CPU time as a function of the number of

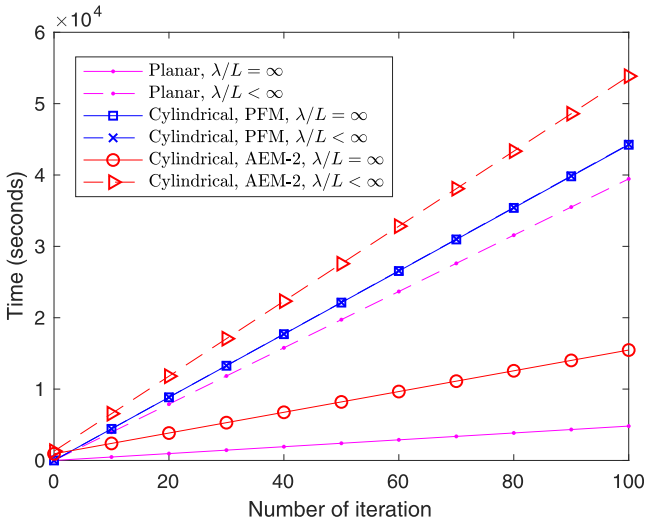

Figure 3. Comparison of the CPU time of the PFM and the AEM (up to the second-order expansion). The numerical parameters are $N_x = 400$ and $N_s = 800$.

iterations for both the PFM and the AEM. It is evident that the AEM is about 2 times faster than the PFM for one iteration when the semiflexible blocks are rigid rods ($\lambda/L = \infty$). This is because the MDE in the PFM contains orientation operators (L_{CS}) introduced by the curvatures, which is time-consuming and needs to be computed at each iteration. In contrast, for the AEM, the operator L_{CS} appears in the source term and only needs to be computed once. However, one iteration in the AEM is a little slower than that of the PFM when the chains are semiflexible ($\lambda/L < \infty$). Note that using the PFM, we need to solve the SCFT model many times (25 times, for example, determined by how many curvature values that we need to be constrained at). Therefore, the total number of iteration is much large than that of the AEM. Generally, the AEM is more efficient than the PFM to calculate the elastic moduli (especially for the rigid rod case).

https://doi.org/10.1021/acs.jpcb.1c01116
J. Phys. Chem. B 2021, 125, 5309−5320

Let us summarize the pros and cons of the PFM and the AEM to calculate the elastic moduli of liquid-crystalline bilayers. The significant merit of the AEM is that it provides an analytical expression of the elastic moduli, which corresponding to a few SCF equations with the MDE, including source terms. Using the analytical expressions, we only need to solve five SCF equations (corresponding to F_0, F_1^C, F_2^C, F_1^S, and F_2^S) to obtain all of the second-order moduli and additional four SCF equations for the fourth-order moduli. In contrast, the PFM needs to solve the SCF equations many times, which is determined by how many curvature values should be used for the polynomial fitting. Although five points of $(c, F_{ex}(c))$ are enough to determine a fourth-order polynomial $F_{ex}(c)$, we should use more points (such as 25 points) to ensure the fitted coefficients are reasonable since the free energies include numerical errors. Therefore, to obtain all of the second- and fourth-order moduli, the PFM needs to solve the SCF equations about 50 times (the cylindrical and spherical bilayers have each 25 times). However, in the AEM, the SCF equations should be solved successively, and the lower-order terms of propagators appear in higher-order source terms of the MDE, which results in an increase of the CPU memory. These comparisons are listed in Table 1.

Table 1. Summary of the PFM and the AEM to Calculate the Elastic Moduli of Liquid-Crystalline Bilayer Membranes

property	PFM	AEM
analytical expression	no	yes
MDE	standard	has source terms
solve SCF equations	~50 times	5–9 times
CPU memory	one instance	two instances

5.2. Decomposition of the Order Parameters. As a merit of the AEM, the order parameters of curved bilayers can be recovered by the asymptotic expansion. Figure 4 gives the decomposition of a spherical bilayer with the curvature $c \approx 0.14$, and the zeroth-, first-, and second-order concentrations in the AEM. For this curvature, the third- and fourth-order concentrations are small (less than 0.1 for ϕ_A^c; see Figure 4d). Note that the zeroth-order and the second-order concentration profiles are symmetric with respect to the center of the bilayer, while the first-order profile is antisymmetric. Hence, the odd-order terms in the free energies can be omitted.

It is interesting to note that the profile of the ith-order concentrations is similar to that of the derivative of the $(i-1)$th-order concentrations (up to a proper multiplier), such as $\phi_{A,1}(x) \approx 1.0\ \phi'_{A,0}(x)$ and $\phi_{A,2}(x) \approx 0.7\ \phi'_{A,1}(x)$ for the example in Figure 4. These relations provide good initializations for solving the high-order SCF equations because we can initialize the $(i+1)$th-order concentrations based on the derivative of the ith-order concentrations.

5.3. Elastic Properties of Semiflexible Bilayers. Now we show some results on the elastic properties of semiflexible bilayer membranes that exhibit liquid-crystalline orders. First, we examine the bending modulus and Gaussian modulus difference between flexible and semiflexible bilayer membranes. To make this comparison, we fix the Flory–Huggins parameter as $\chi N = 30$, turning off the orientational interaction between rods, *i.e.*, letting $\eta N = 0$, setting the geometrical asymmetry parameter $\beta = \sqrt{6}$ such that the rigid rod and coil have the same mean-squared end-to-end vector.[18,30] The results are given in Figure 5, where the elastic moduli of tensionless flexible (coil–coil) and semiflexible (rod-coil) bilayer membranes are shown as a function of the hydrophilic fraction f_A. It is indicated that the flexible bilayers have a higher bending

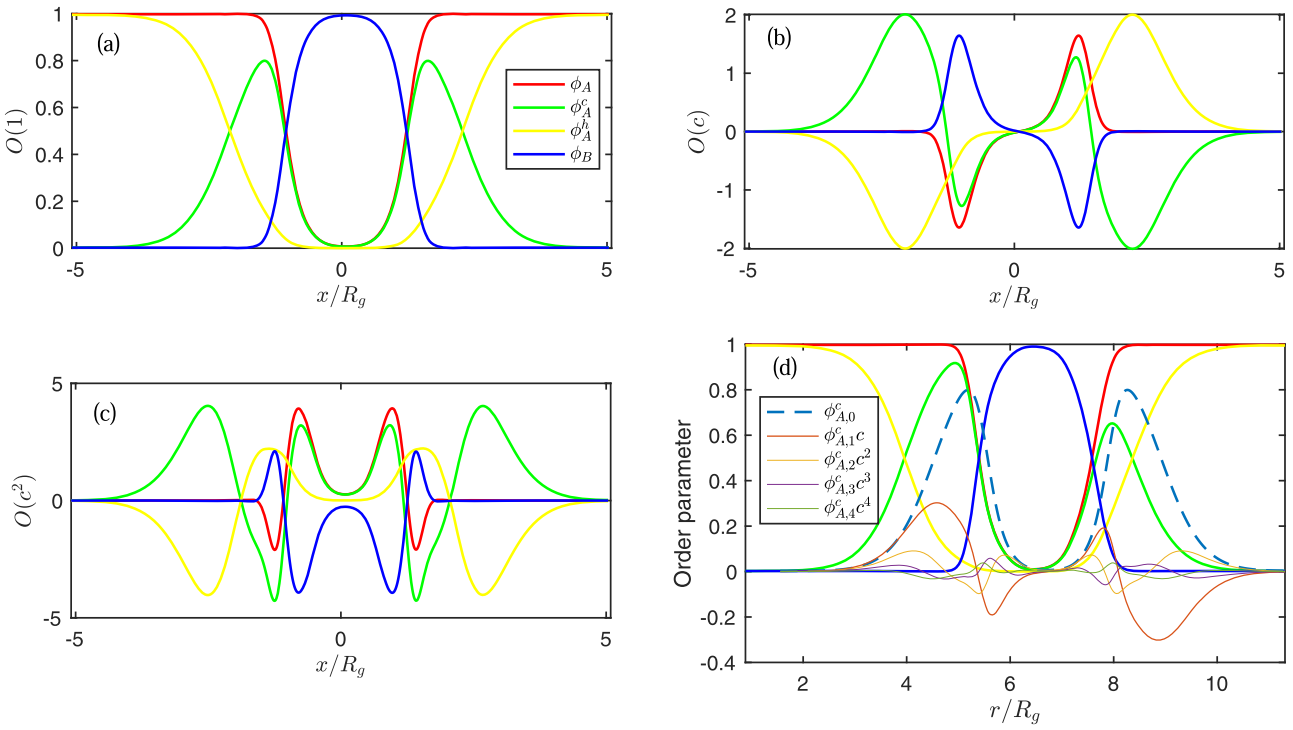

Figure 4. Order parameters of bilayers. (a–c) Local concentrations in AEM at the zeroth, first, and second orders, respectively. (d) Local concentrations of a spherical bilayer with curvature $c \approx 0.14$, and the decomposition of ϕ_A^c up to the fourth-order component. Model parameters are the same as Figure 2.

https://doi.org/10.1021/acs.jpcb.1c01116
J. Phys. Chem. B 2021, 125, 5309–5320

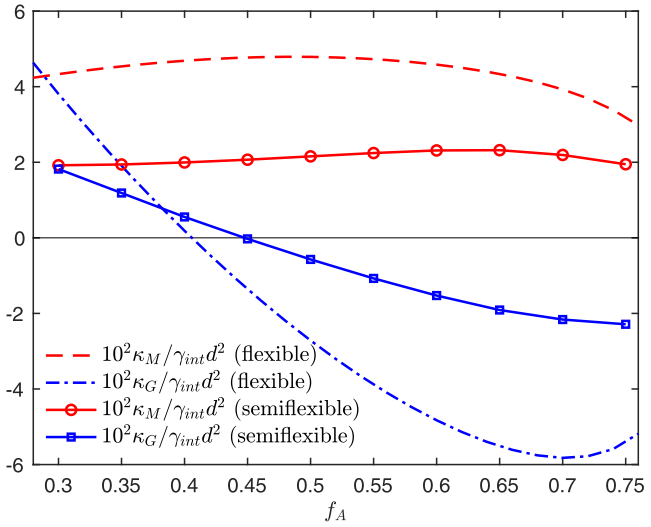

Figure 5. Elastic moduli of tensionless flexible (coil−coil) and semiflexible (rod-coil) bilayer membranes as functions of the hydrophilic fraction f_A with $\chi N = 30$. The unit of elastic moduli is adopted from Li et al.[16] (Other model parameters for rod-coil are $\eta N = 0$, $\beta = \sqrt{6}$, and $\lambda/L = \infty$).

modulus κ_M than semiflexible bilayers (about 1.8 to 2.3 times). The former also has a higher magnitude of Gaussian modulus κ_G. Note that Katsov et al.[15] compared the bending moduli of monolayer (equals $\kappa_M/2$) obtained from SCFT with experimental values and suggested a scale-down factor of about 2.5. This factor is close to 1.8−2.3 and hence implies that modeling the polymer as semiflexible chains might predict the elastic moduli more accurately than flexible chains.

Next, we turn to the effect of model parameters on the elastic properties of tensionless bilayers. Figure 6a gives the second- and fourth-order moduli as functions of f_A with two values of χN ($\chi N = 15$ and $\chi N = 20$). The bending modulus κ_M and the fourth modulus (B_C and B_S) have a weak symmetry around $f_A = 0.5$, and the Gaussian modulus κ_G changes from positive to negative around $f_A = 0.43$. Besides, the magnitude of the moduli increases with increasing Flory−Huggins parameter χN. Figure 6b gives the elastic moduli as functions of ηN. The κ_M and B_C values are positive, while the κ_G and B_S values are negative in most cases. The magnitudes of elastic moduli are roughly increasing functions of ηN; however, their increment is not always smooth since there exist bilayer phase transitions between different liquid-crystalline orders.[24] For the example of $\chi N = 15$, $f_A = 0.5$, the bilayer is in A_n phase for $\eta N = 20$ and in A_s phase for $\eta N = 30$, and the A_n−A_s phase transition occurs about $\eta N = 23$. The tensionless bilayers in the A_s phase have significantly higher moduli than the A_n phase. When ηN is small (less than ∼10), the bilayers' liquid-crystalline order is weak and the elastic moduli hardly changed. In contrast, the liquid-crystalline order with high ηN has significant effects on the elastic properties.

6. CONCLUSIONS

In this paper, we extended the AEM to liquid-crystalline bilayer membranes within the SCFT framework, where the liquid-crystalline order occurs by introducing wormlike chains in the amphiphilic copolymers. Analytic expressions of the elastic moduli of self-assembled liquid-crystalline bilayers are derived and related to a few SCF equations. In contrast, the PFM needs to solve a large number of SCF equations before fitting the energy curves. Since it is time-consuming to solve the MDE for wormlike chains, the PFM has a heavy computing burden. The AEM only needs to solve a few SCF equations to remarkably reduce the computational cost. We have performed the AEM for self-assembled *A* phase bilayers and verified its validity and efficiency.

Although the model and methods are restricted to a rod-coil diblock system, it is straightforward to extend the AEM to other molecular architectures. It is expected that the AEM will contribute to better exploring and understanding the dependence of elastic properties on the molecular architecture and microscopic parameters. In addition, other liquid-crystalline orders such as the *C*-phase bilayers can also become the

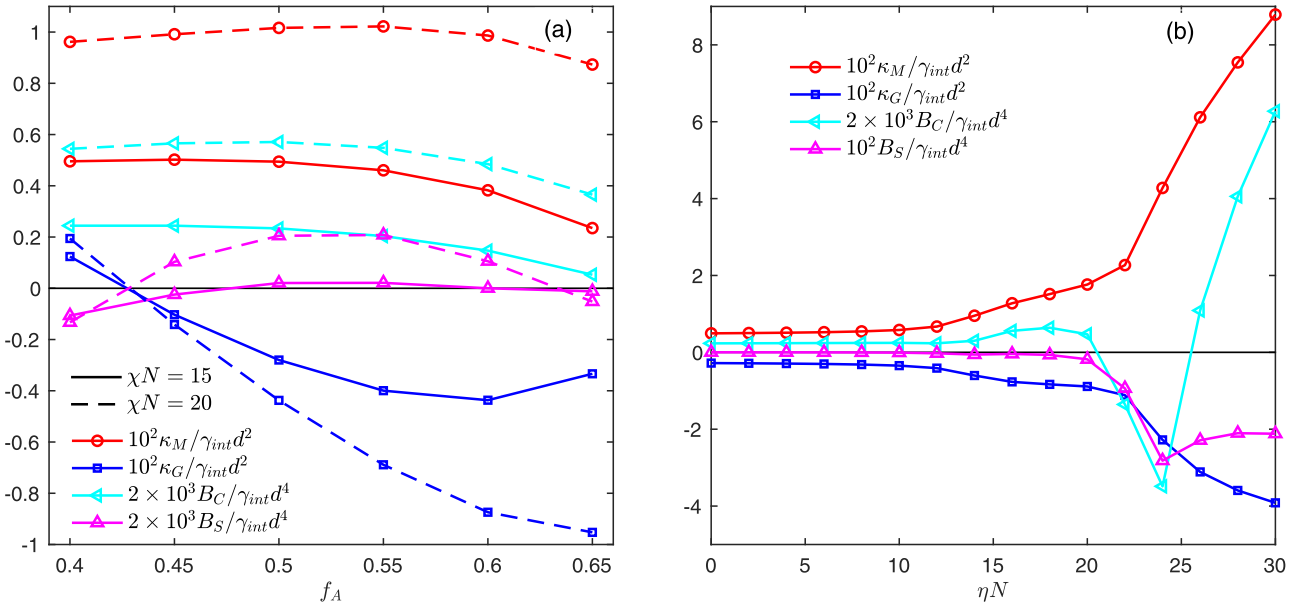

Figure 6. Elastic moduli of tensionless semiflexible bilayer membranes as functions of (a) the hydrophilic fraction f_A and (b) the Maier−Saupe parameter ηN ($\chi N = 15$, $f_A = 0.5$). (Other model parameters: $\beta = \sqrt{6}$ and $\lambda/L = \infty$).

https://doi.org/10.1021/acs.jpcb.1c01116
J. Phys. Chem. B 2021, 125, 5309−5320

equilibrium state for some molecular parameters,[24] and it is interesting to study the effect of molecular tilt on the elastic properties of bilayers, which will be left for our future work.

A. NONUNIFORM GRIDS

To capture the sharp interface of bilayers, we use the nonuniform grid induced by a transformation $t(\zeta)$

$$t(\zeta) = \zeta + kL\left(\frac{1}{2\pi}\sin(2\pi\zeta/L) - \frac{4}{\pi}\cos(\pi\zeta_0/L)\sin(\pi\zeta/L)\right)$$

where ζ_0 is a parameter that corresponds to the position of interfaces and k is a small positive number that controls the nonuniform degree of the grid. A larger k results in a larger nonuniform degree, which means more nodes near the interface. To quantitatively control the nonuniform degree, we define a dense ratio d reflecting how dense the nonuniform grid is over the uniform grid

$$d := \left(\min_{\zeta\in[-L,L]} t'(\zeta)\right)^{-1} = \frac{1}{1 - k(1 + 2\cos^2(\pi\zeta_0/L))}$$

Figure 7 gives examples of nonuniform grid with different degrees, where the computational domain is rescaled to $[-1, 1]$ and ζ_0 is adjusted to capture interfaces at $x = \pm 0.25$. Note that the dense ratio $d = 2$ indicates that the grid at $x = \pm 0.25$ is double dense as the uniform grid. In our numerical experiments, the nonuniform dense ratio is set as $d = 1.5$.

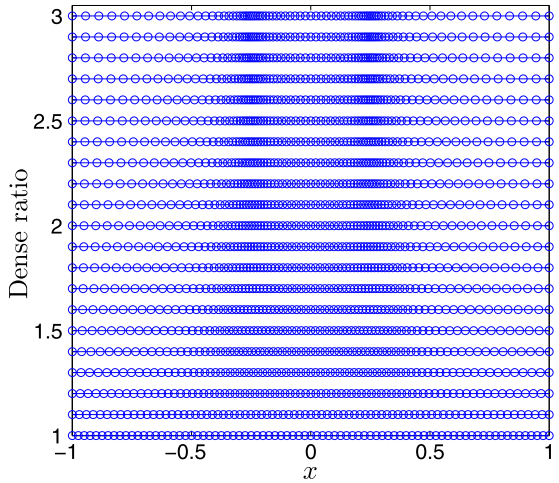

Figure 7. Examples of grid with different nonuniform degrees controlled by the dense ratios.

B. OPERATIONS ON SPHERICAL HARMONICS

The spherical harmonics are defined as

$$Y_l^m(\Theta, \Phi) = \sqrt{\frac{2l+1}{4\pi}\frac{(l-m)!}{(l+m)!}}P_l^m(\cos\Theta)e^{im\Phi},\quad |m| \le l,\ l \ge 0$$

where P_l^m denotes the associated Legendre polynomials. The spherical harmonics are eigenfunctions of the Laplacian operator, $\nabla_{\mathbf{u}}^2$, and have the relation: $\nabla_{\mathbf{u}}^2 Y_l^m = -l(l+1)Y_l^m$. When the operator L_{CS} in cylindrical and spherical coordinates (*i.e.*, L_C and L_S) act on Y_l^m, the results $L_{CS}Y_l^m$ can be expressed by several spherical harmonics[24]

$$L_C Y_l^m = a_{lm}^- Y_{l-1}^m + a_{lm}^+ Y_{l+1}^m + b_{lm}^- Y_{l-1}^{m-2} + b_{lm}^+ Y_{l+1}^{m-2} + c_{lm}^- Y_{l-1}^{m+2} + c_{lm}^+ Y_{l+1}^{m+2} \quad (46)$$

$$L_S Y_l^m = 2a_{lm}^- Y_{l-1}^m + 2a_{lm}^+ Y_{l+1}^m \quad (47)$$

Here, $Y_l^m = 0$ for $l < 0$ or $|m| > l$, and the coefficients are

$$a_{lm}^- = \frac{l+1}{2}\sqrt{\frac{l^2-m^2}{4l^2-1}},\quad a_{lm}^+ = -\frac{l}{2}\sqrt{\frac{(l+1)^2-m^2}{4(l+1)^2-1}},$$

$$b_{lm}^- = -\frac{1}{4}\sqrt{\frac{(l-m+1)(l+m-2)(l+m-1)(l+m)}{4l^2-1}},$$

$$b_{lm}^+ = \frac{1}{4}\sqrt{\frac{(l-m+1)(l-m+2)(l-m+3)(l+m)}{4(l+1)^2-1}},$$

$$c_{lm}^- = -\frac{1}{4}\sqrt{\frac{(l+m+1)(l-m-2)(l-m-1)(l-m)}{4l^2-1}},$$

$$c_{lm}^+ = \frac{1}{4}\sqrt{\frac{(l+m+1)(l+m+2)(l+m+3)(l-m)}{4(l+1)^2-1}}$$

C. UPDATE THE FIELDS

With old fields $\omega_{Ai}^{old}(x)$, $\omega_{Bi}^{old}(x)$, and $\mathbf{M}_i^{old}(x)$ (and its corresponding concentrations $\phi_{Ai}^{old}(x)$, $\phi_{Bi}^{old}(x)$, and $\mathbf{S}_i^{old}(x)$) in hand, we update the fields by the iteration

$$\omega_{Ai}^{new}(x) = (1-\alpha_1)\omega_{Ai}^{old}(x) + \alpha_1\left[\chi N\phi_{Bi}^{old}(x) - \xi_i^{old}(x) + \sum_{j=0}^{i}\psi_j^{old}G_{\varepsilon,i-j}(x-h_0)\right],$$

$$\omega_{Bi}^{new}(x) = (1-\alpha_1)\omega_{Bi}^{old}(x) + \alpha_1\left[\chi N\phi_{Ai}^{old}(x) - \xi_i^{old}(x) - \sum_{j=0}^{i}\psi_j^{old}G_{\varepsilon,i-j}(x-h_0)\right],$$

$$\mathbf{M}_i^{new}(\mathbf{r}) = (1-\alpha_2)\mathbf{M}_i^{old}(\mathbf{r}) + \alpha_2\eta N\mathbf{S}_i^{old}(\mathbf{r})$$

where α_i, $i = 1, 2$, are update ratios, which are chosen as $\alpha_1 = 0.03$ and $\alpha_2 = 0.01$ in our calculations. This is the Picard-type iteration which is robust but converges slowly. Therefore, when the fields are updated by a lot of Picard iterations such that the error is less than 0.1, we turn to the Anderson iteration where the corresponding fixed point problem is eqs 36−38. In both the Picard and Anderson iterations, the Lagrange field $\xi_i(x)$ and ψ_i are given by (omit the superscript)

$$\xi_i(x) = \frac{1}{2}(\chi N(\phi_{Ai}(x) + \phi_{Bi}(x)) - (\omega_{Ai}(x) + \omega_{Bi}(x))) - \gamma\chi N(\phi_{Ai}(x) + \phi_{Bi}(x) - \delta_{0i}),$$

$$\psi_i = \left[\int x(\omega_{Ai}(x) - \omega_{Bi}(x) - \chi N(\phi_{Bi}(x) - \phi_{Ai}(x)) - 2\sum_{j=0}^{i-1}\psi_j G_{\varepsilon,i-j}(x-h_0))dx - \beta\chi N I_{\psi,i}\right] / \left[2\int xG_\varepsilon(x-h_0)dx\right]$$

https://doi.org/10.1021/acs.jpcb.1c01116
J. Phys. Chem. B 2021, 125, 5309−5320

where γ and β are numerical parameters, which are chosen as 0.6 and 0.4, respectively. Note that the constraint eq 41 is satisfied because of the existence of field ψ_i; hence, $I_{\psi i}$ appears in the iteration.

AUTHOR INFORMATION

Corresponding Author

Yongqiang Cai − *School of Mathematical Sciences, Laboratory of Mathematics and Complex Systems, MOE, Beijing Normal University, 100875 Beijing, China;* orcid.org/0000-0002-2666-0539; Email: caiyq.math@bnu.edu.cn

Authors

Xiaoyuan Wang − *School of Mathematics and Statistics, Guizhou University, 550025 Guiyang, China*

Sirui Li − *School of Mathematics and Statistics, Guizhou University, 550025 Guiyang, China; School of Mathematical Sciences, Zhejiang University, 310027 Hangzhou, China*

Complete contact information is available at: https://pubs.acs.org/10.1021/acs.jpcb.1c01116

Notes

The authors declare no competing financial interest.

ACKNOWLEDGMENTS

We thank anonymous reviewers for their valuable comments and useful suggestions. This research was supported by the Fundamental Research Funds for the Central Universities, the NSF of China under grant no. 12061019 and by the Growth Foundation for Youth Science and Technology Talent of Educational Commission of Guizhou Province of China under grant no. [2021]087.

REFERENCES

(1) Taubert, A.; Napoli, A.; Meier, W. Self-assembly of Reactive Amphiphilic Block Copolymers As Mimetics for Biological Membranes. *Curr. Opin. Chem. Biol.* **2004**, *8*, 598−603.

(2) Helfrich, W. Elastic properties of lipid bilayers: theory and possible experiments. *Z. Naturforsch., C* **1973**, *28*, 693−703.

(3) Tu, Z.; Ou-Yang, Z. Recent theoretical advances in elasticity of membranes following Helfrich's spontaneous curvature model. *Adv. Colloid Interface Sci.* **2014**, *208*, 66−75.

(4) Nagle, J. Introductory Lecture: Basic Quantities in Model Biomembranes. *Faraday Discuss.* **2013**, *161*, 11−29.

(5) Dimova, R. Recent Developments in the Field of Bending Rigidity Measurements on Membranes. *Adv. Colloid Interface Sci.* **2014**, *208*, 66−75.

(6) Thakkar, F. M.; Maiti, P. K.; Kumaran, V.; Ayappa, K. G. Verifying scalings for bending rigidity of bilayer membranes using mesoscale models. *Soft Matter* **2011**, *7*, 3963−3966.

(7) Sodt, A. J.; Pastor, R. W. Bending free energy from simulation: correspondence of planar and inverse hexagonal lipid phases. *Biophys. J.* **2013**, *104*, 2202−2211.

(8) Hu, M.; Briguglio, J.; Deserno, M. Determining the Gaussian curvature modulus of lipid membranes in simulations. *Biophys. J.* **2012**, *102*, 1403−1410.

(9) Berthault, A.; Werner, M.; Baulin, V. A. Bridging molecular simulation models and elastic theories for amphiphilic membranes. *J. Chem. Phys.* **2018**, *149*, No. 014902.

(10) Marsh, D. Elastic curvature constants of lipid monolayers and bilayers. *Chem. Phys. Lipids* **2006**, *144*, 146−159.

(11) Zhang, P.-W.; Shi, A.-C. Application of Self-consistent Field Theory to Self-assembled Bilayer Membranes. *Chin. Phys. B* **2015**, *24*, No. 128707.

(12) Kheyfets, B.; Galimzyanov, T.; Drozdova, A.; Mukhin, S. Analytical calculation of the lipid bilayer bending modulus. *Phys. Rev. E* **2016**, *94*, No. 042415.

(13) Cai, Y.; Li, S.; Shi, A.-C. Elastic properties of self-assembled bilayer membranes: Analytic expressions via asymptotic expansion. *J. Chem. Phys.* **2020**, *152*, No. 244121.

(14) Müller, M.; Gompper, G. Elastic properties of polymer interfaces: aggregation of pure diblock, mixed diblock, and triblock copolymers. *Phys. Rev. E* **2002**, *66*, No. 041805.

(15) Katsov, K.; Müller, M.; Schick, M. Field theoretic study of bilayer membrane fusion. I. Hemifusion mechanism. *Biophys. J.* **2004**, *87*, 3277−3290.

(16) Li, J.; Pastor, K.; Shi, A.-C.; Schmid, F.; Zhou, J. Elastic Properties and Line Tension of Self-assembled Bilayer Membranes. *Phys. Rev. E* **2013**, *88*, No. 012718.

(17) Xu, R.; Dehghan, A.; Shi, A.-C.; Zhou, J. Elastic property of membranes self-assembled from diblock and triblock copolymers. *Chem. Phys. Lipids* **2019**, *221*, 83−92.

(18) Cai, Y.; Zhang, P.; Shi, A.-C. Elastic properties of liquid-crystalline bilayers self-assembled from semiflexible-flexible diblock copolymers. *Soft Matter* **2019**, *15*, 9215−9223.

(19) Yang, G.; Tang, P.; Yang, Y.; Wang, Q. Self-assembled Microstructures of Confined Rod-coil Diblock Copolymers by Self-consistent Field Theory. *J. Phys. Chem. B* **2010**, *114*, 14897−14906.

(20) Olsen, B. D.; Segalman, R. A. Self-assembly of Rod-coil Block Copolymers. *Mater. Sci. Eng., R* **2008**, *62*, 37−66.

(21) Lim, Y.-B.; Moon, K.-S.; Lee, M. Rod-coil Block Molecules: Their Aqueous Self-assembly and Biomaterials Applications. *J. Mater. Chem.* **2008**, *18*, 2909−2918.

(22) Zhang, J.; Chen, X.-F.; Wei, H.-B.; Wan, X.-H. Tunable Assembly of Amphiphilic Rod-coil Block Copolymers in Solution. *Chem. Soc. Rev.* **2013**, *42*, 9127−9154.

(23) Shi, L.-Y.; Zhou, Y.; Fan, X.-H.; Shen, Z. Remarkably Rich Variety of Nanostructures and Order-order Transitions in a Rod-coil Diblock Copolymer. *Macromolecules* **2013**, *46*, 5308−5316.

(24) Cai, Y.; Zhang, P.; Shi, A.-C. Liquid crystalline bilayers self-assembled from rod-coil diblock copolymers. *Soft Matter* **2017**, *13*, 4607−4615.

(25) Song, W.; Tang, P.; Qiu, F.; Yang, Y.; Shi, A.-C. Phase Behavior of Semiflexible-coil Diblock Copolymers: A Hybrid Numerical Scft Approach. *Soft Matter* **2011**, *7*, 929−938.

(26) Yu, J.; Liu, F.; Tang, P.; Qiu, F.; Zhang, H.; Yang, Y. Effect of Geometrical Asymmetry on the Phase Behavior of Rod-coil Diblock Copolymers. *Polymers* **2016**, *8*, 184.

(27) Flory, P. *Principles of Polymer Chemistry*; Cornell University Press: Ithaca, New York, 1953.

(28) Maier, W.; Saupe, A. A Simple Molecular Theory of the Nematic Crystalline-liquid State. *Z. Naturforsch., A* **1958**, *13*, 564−566.

(29) Matsen, M. Elastic properties of a diblock copolymer monolayer and their relevance to bicontinuous microemulsion. *J. Chem. Phys.* **1999**, *110*, 4658−4667.

(30) Fredrickson, G. H. *The Equilibrium Theory of Inhomogeneous Polymers*; Oxford University Press: Oxford, 2006.

(31) Laradji, M.; Desai, R. C. Elastic Properties of Homopolymer-homopolymer Interfaces Containing Diblock Copolymers. *J. Chem. Phys.* **1998**, *108*, 4662−4674.

(32) Holmes, M. H. *Introduction to Perturbation Methods*; Springer Science & Business Media, 2012; Vol. *20*.

(33) Neu, J. C. *Singular Perturbation in the Physical Sciences*; American Mathematical Society, 2015; Vol. *167*.

(34) Strang, G. On the construction and comparison of difference schemes. *SIAM J. Numer. Anal.* **1968**, *5*, 506−517.

(35) Morton, K. W.; Mayers, D. F. *Numerical Solution of Partial Differential Equations: An Introduction*, 2nd ed.; Cambridge University Press, 2005.

(36) Lele, S. K. Compact finite difference schemes with spectral-like resolution. *J. Comput. Phys.* **1992**, *103*, 16−42.

(37) Butcher, J. C. *Numerical Methods for Ordinary Differential Equations*, 2nd ed.; Springer-Verlag, 2008.
(38) Thompson, R. B.; Rasmussen, K. O.; Lookman, T. Improved Convergence in Block Copolymer Self-consistent Field Theory by Anderson Mixing. *J. Chem. Phys.* **2004**, *120*, 31−34.
(39) Bubnis, G.; Risselada, H. J.; Grubmüller, H. Exploiting Lipid Permutation Symmetry to Compute Membrane Remodeling Free Energies. *Phys. Rev. Lett.* **2016**, *117*, No. 188102.

https://doi.org/10.1021/acs.jpcb.1c01116
J. Phys. Chem. B 2021, 125, 5309−5320